Global Teleconnections of Ocean Climate to Terrestrial Carbon Flux

C. Potter [1*], S. Klooster [2], M. Steinbach [3], P. Tan [3],

V. Kumar [3], S. Shekhar [3], R. Nemani [4], R. Myneni [5]

[1] NASA Ames Research Center, Moffett Field, CA

[2] California State University Monterey Bay, Seaside, CA

[3] University of Minnesota, Minneapolis, MN

[4] University of Montana, Missoula, MT

[5] Boston University, Boston, MA

Please return comments and other correspondence to:

[*] Corresponding author at

Email: cpotter@gaia.arc.nasa.gov

Tel. 650-604-6164; Fax. 650-604-4680

Draft Date: June 12, 2002

Submission to: *J. Geophysical Research-Atmospheres*

Abstract. We have applied association analysis to 17 years of ocean climate observations and predicted net ecosystem production on land to infer short-term (monthly to yearly) teleconnections between sea surface temperature and terrestrial carbon cycles. The analysis suggests that, on a global level, ocean climate indices can be used to reliably predict net ecosystem carbon fluxes over more than 58 percent of the non-desert/ice covered land surface, commonly with a lead period of 2-6 months. These strong teleconnections detected between ocean surface climate and seasonal carbon gain in terrestrial vegetation offer important capabilities for making inferences about the variability in the terrestrial carbon cycle of natural and agricultural ecosystems world-wide.

1. Introduction

Net photosynthetic accumulation of carbon by plants, also known as net primary production (NPP), provides the energy that drives most biotic processes on Earth. NPP produces organic matter that is consumed by microbes and animals. Sustained NPP can contribute to unique biological properties of Earth's terrestrial surface, such as the diversity of organisms supported by any given eco-climatic zone. Moreover, climate controls on NPP fluxes are an issue of central relevance to human society, mainly because of concerns about the extent to which NPP in managed ecosystems can provide adequate food and fiber for an exponentially growing population. Predictability in the NPP fluxes of agricultural zones is a principal foundation for sustainable development. In addition, accounting for the potential of long-term entrapment of atmospheric CO_2 derived from fossil fuel pollution sources back in terrestrial ecosystems begins with an understanding of interannual to decadal climate controls on NPP and net ecosystem production (NEP) fluxes, which can further account for terrestrial carbon sinks (Schimel et al., 2001).

As a major biological flux of carbon, predicted NPP for a large land area is a unique integrator of climatic, ecological, geochemical and human influences on the global carbon cycle. In the absence of major human disturbance, surface temperature, solar irradiance, and precipitation have been shown as the strongest controllers of yearly terrestrial NPP at the global scale (Lieth 1975; Mellilo et al. 1993, Potter et al., 1993). Reliable estimates of seasonal NPP and NEP fluxes depend on timely and accurate forecasts of these climate forcing variables over land.

The influence of ocean surface patterns, such as the El Niño-Southern Oscillation (ENSO), on atmospheric circulation and land surface climate have been noted as significant global teleconnections (Glantz et al., 1991). Teleconnection is a term used in meteorological studies to describe simultaneous variation in climate and related processes over widely separated points on earth. There are different phases in ocean climate indices (OCIs) such as the ENSO, which is called El Niño in the warm phase and La Niña in the cold phase. ENSO warming at the sea surface, which is driven by changes in winds and ocean-atmosphere heat exchange, typically extends to about 30°N and 30°S latitude, with lags into continental land areas of several months. Certain elements of climate variability at relatively high latitudes may be predictable from forcings by sea surface temperature (SST) and sea level pressure (SLP) in the tropical ocean (Ting et al., 1996; Hoerling et al., 2001). For example, in the extratropics of the Northern Hemisphere, the deep Aleutian low that accompanies El Niño can advect warm moist air along the west coast of North America bringing warm spells to western Canada and Alaska (Trenberth and Hurrell, 1994). On the time scale of several decades, ENSO can account for 0.06° C of global warming from 1950-1998 (Trenberth et al., 2001).

Previous studies have identified global connections of interannual SST to land surface properties (Keeling et al., 1995; Myneni et al., 1998; Dai et al., 1998). These analyses have mainly focused on a single OCI. At a strictly regional scale, ENSO events have been linked to weather anomalies and crop production in the continental U. S. (Carlson et al., 1996; Nemani et al., 2001), and streamflow patterns in the Pacific northwest (Hamlet and Lettenmeier, 1999). However, large-scale teleconnections between multiple OCIs and global carbon fluxes have yet to be demonstrated, and may escape ready detection without the aid of spatial-temporal analysis tools designed specifically to uncover such associations, both weak and strong, between time series of SST/SLP anomalies and spatially explicit estimates of carbon fluxes on the land.

We report here on approaches to quantify global teleconnections of ocean indices and terrestrial carbon flux represented by monthly NPP and NEP over the period 1982-1998. The principal science question we address is "Can specific geographic zones of ocean climate observations be used as reliable predictors of carbon flux patterns (NEP interannual variability and extreme events) over large areas of the global land surface?" To interpret these results, it is also necessary to incorporate information on when and where anomalies in NPP and NEP drivers of land surface temperature, solar irradiance, and precipitation are linked to similar patterns in the OCIs .

2. Global Data and Models

Several OCIs are of prime interest in this study of ocean-land teleconnections (Trenberth and Hurrell, 1994). We focus here on the Southern Oscillation Index (SOI), the Arctic Oscillation (AO) index, and two NINO indices. Correlations between these OCI anomalies and monthly gridded SST (Bottomley et al., 1990) for period of 1982-1998 indicate the central areas of the ocean temperature

record that can be closely associated with the indices (Figure 1). SOI is an indicator of atmospheric impacts of ENSO, computed as the standardized difference between SLP measured in Tahiti (17ºS, 149ºW) and Darwin, Australia (13ºS, 131ºE). The AO is derived from 1000 mb height anomalies poleward of 20ºN (Thompson and Wallace, 1998). The NINO1+2 index is used to monitor SST over the eastern tropical Pacific, delineated by the area between 0º-10ºS and 90ºW-80ºW. The NINO4 index is used to monitor SST over the area between 5ºN-5ºS and 160ºE-150ºW.

The SOI and NINO indices are commonly used to document warm-phases in ENSO, which are often associated with above-average temperatures in the northwestern half of the North American continent, and below-average temperatures in the southeastern half (Trenberth and Hurrell, 1994; Klein et al., 1999; McCabe and Dettinger, 1999). There is also a pattern of the warm-phase ENSO associated with above-average precipitation over western coastal South America (Vuille et al., 2000), the southern U. S., and northern Mexico, plus below-average precipitation in south-central Africa, northeastern South America, parts of southern Asia and Australia, and in North America from the Canadian Rockies to the Great Lakes region.

The AO is similar in many respected to the North Atlantic Oscillation (NAO – measured between the Icelandic low (65ºN, 22ºW) and the Azores high pressure centers from 39ºN, 9ºW to 36ºN, 6ºW ; Walker and Bliss, 1932), which can represent the persistence of below-average temperatures variations over North Africa and the Middle East, and above-average temperatures over North America. During winters when the NAO index is high, anomalously low precipitation commonly occurs over the Canadian Arctic, central and southern Europe, the Mediterranean and Middle East. In contrast, anomalously high precipitation occurs from Iceland though Scandinavia (Hurrell, 1995).

For this analysis with OCI teleconnections, terrestrial NPP and NEP fluxes have been computed monthly (over the period 1982-1998) at a spatial resolution of 0.5º lat/lon using the NASA-CASA (Carnegie-Ames-Stanford) Biosphere model (Potter, 1999; Potter et al., 1999). NASA-CASA is a numerical model of monthly fluxes of water, carbon, and nitrogen in terrestrial ecosystems. Our estimates of terrestrial NPP fluxes depend on inputs of global satellite observations for land surface properties and on gridded climate drivers from interpolated weather station records (New et al., 2000) distributed across all the continental masses. Consequently, the NASA-CASA predictions of terrestrial NPP carbon fluxes are derived with no dependence whatsoever on ocean climate data, nor on atmospheric circulation model predictions of surface climate patterns.

Our fundamental approach to estimating NPP is to define optimal metabolic rates for carbon fixation processes, and to adjust these rate values using scalars related to the limiting effects of solar radiation, air temperature (TEMP), precipitation (PREC) (New et al., 2000), predicted soil moisture, and land cover (DeFries et al., 1994). Carbon (CO_2) fixed by vegetation as NPP is estimated in the ecosystem model according to the fraction of photosynthetically active radiation (FPAR) intercepted by plant canopies and a light utilization efficiency term (e_{max}). This product is modified by stress scalars for temperature (Ta) and moisture (W) that vary over time and space. The e_{max} term is set uniformly at 0.39 g C MJ^{-1} PAR (Potter et al., 1993), a value that has been validated globally by comparing predicted annual NPP to more than 1900 field estimates of NPP (Figure 2). Interannual NPP fluxes from the CASA model have been reported (Behrenfeld et al., 2001) and validated against multi-year estimates of NPP from field stations and tree rings (Malmström et al., 1997).

Our NASA-CASA model is designed to couple seasonal patterns of NPP to soil heterotropic respiration (R_h) of CO_2 from soils worldwide (Potter, 1999). First-order decay equations simulate exchanges of decomposing plant residue (metabolic and structural fractions) at the soil surface. The model also simulates surface soil organic matter (SOM) fractions that presumably vary in age and chemical composition. Turnover of active (microbial biomass and labile substrates), slow (chemically protected), and passive (physically protected) fractions of the SOM are represented. NEP can be computed as NPP minus total R_h fluxes, excluding the effects of small-scale fires and other localized disturbances or vegetation regrowth patterns on carbon fluxes (Schimel et al., 2001).

Whereas previous versions of the NASA-CASA model (Potter et al., 1993 and 1999) used a normalized difference vegetation index (NDVI) to estimate FPAR, the current model version instead relies upon canopy radiative transfer algorithms (Knyazikhin et al., 1998), which are designed to generate improved FPAR products as inputs to carbon flux calculations. These radiative transfer algorithms, developed for the MODIS (MODerate resolution Imaging Spectroradiometer) aboard the NASA Terra platform, account for attenuation of direct and diffuse incident radiation by solving a three-dimensional formulation of the radiative transfer process in vegetation canopies. Monthly composite data from channels 1 and 2 of the Advanced Very High Resolution Radiometer (AVHRR) have been processed according to the MODIS radiative transfer algorithms and aggregated over the global land surface to 0.5^o resolution, consistent with the NASA-CASA climate driver data.

3. Land Climate Controls on Ecosystem Carbon Fluxes

Association rule analysis can offer useful insights into the types of dependencies that exist among variables within a large data set. Non-random associations between two or more model variables

are reported here using the chi-square test (Stockburger 1998). Chi-square values greater than 3.84 (degrees of freedom=1) indicate a high probability ($p<0.05$) of non-random association between anomalously low (LO) or anomalously high (HI) monthly events for TEMP or PREC with either NPP or NEP. We used an anomalous event threshold value of 1.5 standard deviations or greater from the long-term (1982-1998) monthly mean value. For our analysis, association patterns are reported below on the basis of frequency of occurrence within major global vegetation types (DeFries et al., 1994).

We find that one of the strongest non-random associations in our NASA-CASA results is that PREC-LO events co-occur with NPP-LO and with NEP-LO events in evergreen broadleaf forests, deciduous broadleaf forests, croplands, and grassland savannas (Figure 3a). These events occur mainly in drought-sensitive areas of tropical and sub-tropical zones, and possibly in areas of major wild fires that are associated with FPAR-LO events. We also find that TEMP-HI events co-occur with NPP-LO events for these same vegetation types, which can be another indicator of drought stress effects on plant carbon gains.

Another non-random association rule indicates that TEMP-HI events co-occur with NPP-HI and NEP-HI events in tundra, grasslands, deciduous needleleaf forests, evergreen needleleaf forests, and mixed (needleleaf-broadleaf) forests (Figure 3b), even with co-occurring PREC-LO events. These observations lead to the hypothesis that regional climate warming has had the greatest impact on high latitude (tundra and boreal) sinks for atmospheric CO_2, particularly over the Eurasian continent.

We find in addition that PREC-HI plus TEMP-HI events co-occur with NPP-HI and NEP-HI events in mixed forests, deciduous broadleaf forests, and evergreen needleleaf forests. This non-random

association suggests an important dual control over net carbon fluxes by PREC and TEMP events in transition zones between cool temperate and warmer sub-tropical forest ecosystems.

4. Time Series Teleconnections

Using matching monthly records for the period of 1982-1998, close associations between the time series anomalies of the OCIs and carbon fluxes on land were identified using Pearson's correlation coefficient (r). Examples of the close association between three OCIs and land NPP fluxes at $r>0.4$ are shown in Figure 4. These locations were selected because of their close proximity to land areas where OCI-NPP correlations of $r>0.5$ are aggregated. Both the SOI and NPP fluxes (eastern Brazil) show low points in 1983, 1987,1992, and 1998. The NINO1+2 index and NPP fluxes (southwestern U.S.) both show high points during these same years, suggesting a reverse effect (compared to SOI) of precipitation patterns between the two distant land areas. The AO index and NPP fluxes (southern Scandinavia) both show rapid increases in 1986, 1989 and 1995, which can be attributed to increasing precipitation and temperature on land during these transition periods. We find that a seasonal phase shift in OCI lead times of up to six months commonly improved correlations with the NPP time series anomalies.

Serial correlation (i.e., autocorrelation) needs to be considered when testing significance of the association between two time series. We determined the serial correlation of ocean indices at all possible lag times. SOI anomalies have a low autocorrelation function (< 0.3) at lag times greater than about 6 months (using index data from 1958-1995). The same is true for the NINO1+2 index anomalies. For the NAO/AO anomalies, the autocorrelation function is < 0.1 at lag times greater than 3 months. For our predicted NPP anomalies, the autocorrelation function is < 0.1 at lag times greater than 6 months. Based on these results, we accepted degrees of freedom (df) for the OCI time series

correlations with NPP fluxes to be df=32 (34 'seasons' of 6 months duration in a 17-year window, minus 2 for a 2-tailed test of significance).

For the purposes of demonstrating a significant association of predicted NEP and NPP from NASA-CASA with measured OCI values with df=32, $r > 0.34$ carries a relatively high confidence level of $p<0.05$. Global correlation maps (Figures 5a-c) show the areas where $r>0.34$ for associations of the SOI, NINO1+2, and AO indices with our predicted NEP fluxes for the period 1982-98. Seasonality in all time series records was removed before this analysis by computing a 12-month moving average. Phase shifts (in months) are shown (Figures 5d-f) for the strongest OCI association shown in the correlation maps.

We find that for 58 percent of the global non-barren (desert/ice coverage) of the land, anomalies in deseasonailzed NEP fluxes have significant teleconnections with ocean climate, as represented by four OCI (SOI, AO, NINO1+2, and NINO4) associations combined. The desert and ice-covered areas excluded from our analysis were defined according to the global land cover from DeFries et al. (1994). Each of the four OCIs used to map significant correlations with NEP contributed about 14 percent to the overall non-barren coverage. For deseasonailzed NPP anomalies, 56 percent of the non-barren land surface has a significant teleconnection with the four OCIs. In comparison these NASA-CASA model outputs, the FPAR input time series of deseasonailzed anomalies have significant teleconnections with the four OCIs for 55 percent of the non-barren land surface. These results imply that the NASA-CASA model's prediction of NEP includes important teleconnections and climate controls on terrestrial ecosystem processes that are not captured by satellite FPAR inputs alone.

The influences of climatic teleconnections can be observed in predicted annual carbon fluxes over some of the most drought-stressed land areas of the globe. In particular, the SOI and NINO1+2 indices are consistent indicators of interannual NEP fluxes in large sections of central North and South America, western and central Africa, south Asia and Australia. Teleconnections of AO are most strongly predicted with annual NEP fluxes for large sections of western Canada, Scandinavia, central Eurasia, the Mediterranean, southern Africa, and southern Brazil. We note, however, that certain interior land areas of the Northern Hemisphere above 50°N latitude cannot be significantly correlated with any of the four selected OCIs.

When the non-barren surface is separated into cultivated and uncultivated areas, the total area where anomalies in annual NPP or NEP fluxes have significant correlations (r>0.34) with the four OCIs is much lower for cultivated areas at 7% global coverage than for uncultivated areas at >50% global coverage. This comparison implies that carbon fluxes in cultivated areas worldwide are not as closely linked to large-scale climate teleconnections as are carbon fluxes in uncultivated 'natural' ecosystems.

This first global analysis of ocean climate teleconnections with terrestrial carbon fluxes from satellite observations suggests a number of important lines of study for carbon cycle science. We are able to make an initial assessment of the ecosystem areas that are most strongly influenced by climate teleconnections to ocean processes, thereby laying the foundation for more predictive model development at the global level. The results presented here also begin to demonstrate the magnitude of temporal and spatial variability in terrestrial exchanges of CO_2 with the atmosphere that can be attributed mainly to large-scale coupling of the ocean processes to land climate patterns. Our terrestrial ecosystem model includes predictions for the amount of NPP carbon stored in vegetation biomass and

soils (Potter, 1999; Potter et al., 2001), which makes is possible to link localized controls on atmospheric CO_2 sinks on the land to ocean dynamics anywhere on the globe. With an extension of our predicted terrestrial NPP record from the NASA-CASA model to more than 20 years, additional events in SST/SLP variation can be included in an attempt to establish even stronger ocean-land teleconnections in the carbon cycle. For future studies of the terrestrial carbon cycle, major anomalies in ecosystem carbon fluxes to or from the pool of CO_2 in the atmosphere might be predicted based on more detailed association and statistical analyses of these kind of ocean teleconnections.

Acknowledgments. This work was supported by grants from NASA programs in Intelligent Systems and Intelligent Data Understanding, and the NASA Earth Observing System (EOS) Interdisciplinary Science Program. We thank Joseph Coughlan and David Peterson of NASA Ames Research Center for helpful comments on an earlier version of the manuscript.

References

Behrenfeld, M. J., J. T. Randerson, C. R. McClain, G. C. Feldma, S. Q. Los, C. I. Tucker, P. G. Falkowski, C. B. Field, R. Frouin, W. E. Esaias, D. D. Kolber, and N. H. Pollack, Biospheric primary production during an ENSO transition. *Science* 291, 2594-2597, 2001.

Bottomley, M., C. K. Folland, J. Hsiung, R. E. Newell, and D. E. Parker, Global ocean surface temperature atlas "GOSTA". Meteorological Office, Bracknell, UK and the Department of Earth, Atmospheric and Planetary Sciences, Massachusetts Institute of Technology, Cambridge, MA, USA. 20 pp. , 1990.

Carlson, R. E., D. P. Todey and S. E. Taylor, Midwestern corn yield and weather in relation to extremes of the Southern Oscillation, *J. Prod. Agric.,* 9, 347-352, 1996.

Dai, A., K. E. Trenberth, and T. R. Karl, Global variations in droughts and wet spells: 1900-1995, *Geophys. Res. Lett.,* 25, 3367-3370, 1998.

DeFries, R. and J. Townshend, NDVI-derived land cover classification at global scales, *Internl. J. Remote Sensing*, 15, 3567-3586, 1994

Glantz, M. H., R. W. Katz and N. Nicholls (eds.), *Teleconnections linking world-wide climate anomalies*. Cambridge University Press, New York, 527 p., 1991.

Hamlet, A. F. and D. P. Lettenmeier, Columbia River streamflow forecasting based on ENSO and PDO climate signals, *Am. Soc. Civil. Engin.,* 25, 333-341, 1999.

Hurrell, J. W., Decadal trends in the North Atlantic Oscillation regional temperatures and precipitation, *Science*, 269, 676-679, 1995.

Hoerling, M. P., J. W. Hurrell, and T. Xu, Tropical origins for recent North Atlantic climate change, *Science*, 292, 90-92. 2001.

Keeling, C. D., T. P. Whorf, M. Whalen, and J. van der Plicht, Interannual extremes in the rise of atmospheric carbon dioxide since 1980, *Nature*, 375, 666-66, 1995.

Klein, S. A., B. J. Soden, and N-C. Lau, Remote sea surface temperature variations during ENSO: Evidence for a tropical atmospheric bridge, *J. Climate,* 12, 917-932, 1999.

Knyazikhin, Y., J. V. Martonchik, R. B. Myneni, D. J. Diner, and S. W. Running, Synergistic algorithm for estimating vegetation canopy leaf area index and fraction of absorbed photosynthetically active radiation from MODIS and MISR data, *J. Geophys. Res.*, 103, 32,257-32,276, 1998.

Lieth, H., Modeling the primary productivity of the world. Pages 237-263 in H. Lieth, and R. H. Whittaker, editors. *Primary Productivity of the Biosphere*. Springer-Verlag, Berlin, 1975.

Malmström, C. M., M. V. Thompson. G. P. Juday, S. O. Los, J. T. Randerson, and C. B. Field, Interannual variation in global scale net primary production: Testing model estimates. *Global Biogeochem. Cycles*. 11, 367-392, 1997.

McCabe, G. J. and M. D. Dettinger, Decadal variations in the strength of ENSO teleconnections with precipitation in the western United States. *Internl. J. Climatol.,* 19, 1399-1410, 1999.

Melillo J. M., A. D. McGuire, D. W. Kicklighter, B. Moore III, C. J. Vorosmarty, and A. L. Schloss, Global climate change and terrestrial net primary production, *Nature*, 363, 234-240, 1993.

Myneni, R. B., C. J. Tucker, G. Asrar, and C. D. Keeling, Interannual variations in satellite-sensed vegetation index data from 1981 to 1991, *J. Geophys. Res*., 103, 6145-6160, 1998.

Nemani, R. R., M. A. White, D. R. Cayan, G. V. Jones, S. W. Running, and J. C. Coughlan, Asymmetric climatic warming improves California vintages, *Climate Research*, 19, 25-34, 2001

New, M., M. Hulme, and P. Jones, Representing twentieth century space-time climate variability. II. Development of 1901-1996 monthly grids of terrestrial surface climate, *J. Climate* , 13, 2217-2238, 2000.

Potter, C. S., Terrestrial biomass and the effects of deforestation on the global carbon cycle. *BioScience*, 49, 769-778, 1999.

Potter, C. S., V. Brooks-Genovese, S. A. Klooster, M. Bobo, and A. Torregrosa, Biomass burning losses of carbon estimated from ecosystem modeling and satellite data analysis for the Brazilian Amazon region. *Atmos. Environ.,* 35, 1773-1781, 2001.

Potter, C. S., S. A. Klooster, and V. Brooks, Interannual variability in terrestrial net primary production: Exploration of trends and controls on regional to global scales, *Ecosystems,* 2, 36-48, 1999.

Potter, C. S., J. T. Randerson, C. B. Field, P. A. Matson, P. M. Vitousek, H. A. Mooney, and S. A. Klooster, Terrestrial ecosystem production: A process model based on global satellite and surface data, *Global Biogeochem, Cycles.*, 7, 811-841, 1993.

Schimel D, House J, Hibbard K, Bousquet P, Ciais P, Peylin P, Apps M, Baker D, Bondeau A, Brasswell R, Canadell J, Churkina G, Cramer W, Denning S, Field C, Friedlingstein P, Goodale C, Heimann M, Houghton RA, Melillo J, Moore III B, Murdiyarso D, Noble I, Pacala S, Prentice C, Raupach M, Rayner P, Scholes B, Steffen W, Wirth C, Recent patterns and mechanisms of carbon exchange by terrestrial ecosystems, *Nature*, 414:169-172, 2001.

Stockburger, D. W. Introductory Statistics: Concepts, Models, And Applications, WWW Version 1.0, http://www.psychstat.smsu.edu/sbk00.htm, 1998,

Thompson, D. W. J. and J. M. Wallace, The Arctic Oscillation signature in the wintertime geopotential height and temperature fields, *Geophys. Res. Lett.,* 25, 1297-1300, 1998.

Ting, M., M. P. Hoerling, T.-Y. Xu, and A. Kumar, Northern Hemisphere teleconnection patterns during extreme phases of the zonal mean circulation, *J. Climate,* 9, 2614-2623, 1996.

Trenberth, K. E., J. M. Caron, D. P. Stepaniak and S. Worley, The evolution of ENSO and global atmospheric temperatures,. *J. Geophys. Res.*, in press.

Trenberth and Hurrell, Decadal atmosphere-ocean variations in the Pacific. *Climate Dynamics,* 9, 303-319, 1994.

Vuille, M., R. S. Bradley, and F. Keimig,, Climate variability in the Andes of Ecuador and its relation to tropical Pacific and Atlantic sea surface temperature anomalies. *J. Climate*, 13: 2520-2535, 2000.

Walker, G. T., and E. W. Bliss, World Weather V., *Mem. Roy. Meteor. Soc.*, 4, 53-84, 1932.

Figures and Captions

Figure 1. Areas of SST represented by correlation values of $r > 0.4$ (Pearson's coefficient) in association with the SOI, AO, NINO1+2, and NINO4 indices for the period 1982-1998. Over 65% of global non-ice sea coverage is represented by the four color coverage.

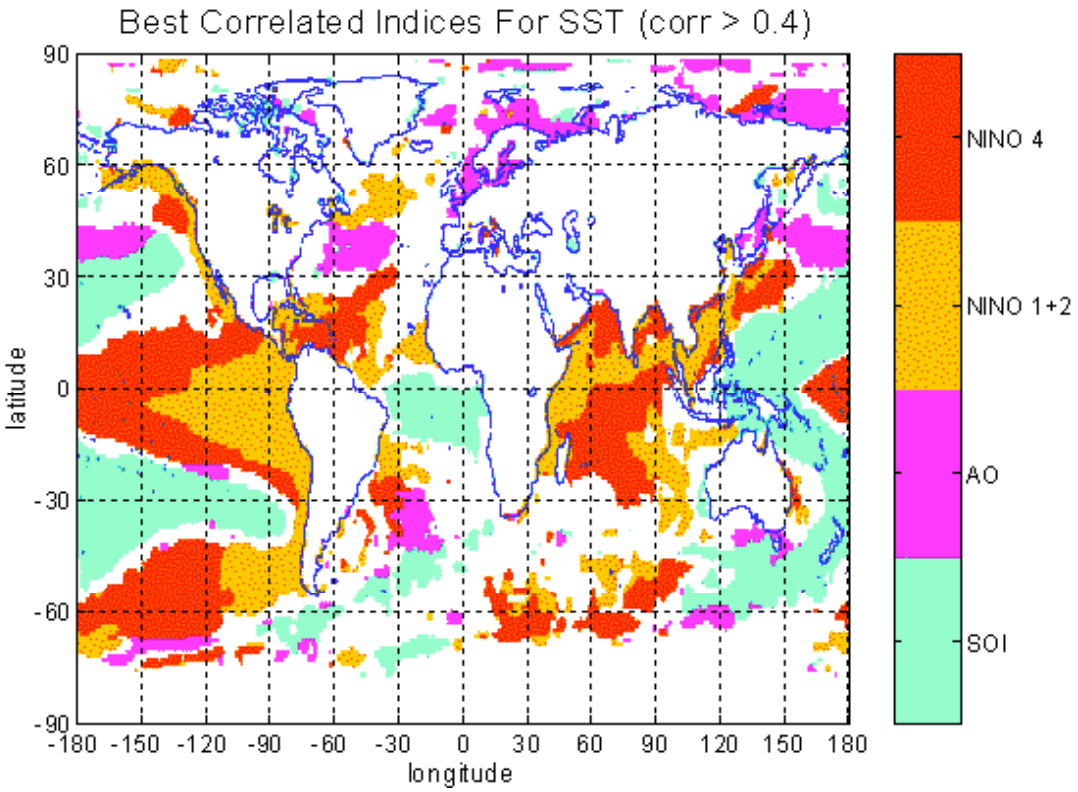

Figure 2. Comparison of annual observed NPP to predicted values from the NASA-CASA model (driven by 0.5º FPAR from the satellite AVHRR and climate means from New et al, 2000). The data set of more than 1900 observed NPP points was compiled for the Ecosystem Model-Data Intercomparison (EMDI) activity by the Global Primary Productivity Data Initiative (GPPDI) working groups of the International Geosphere Biosphere Program Data and Information System (IGBP-DIS).

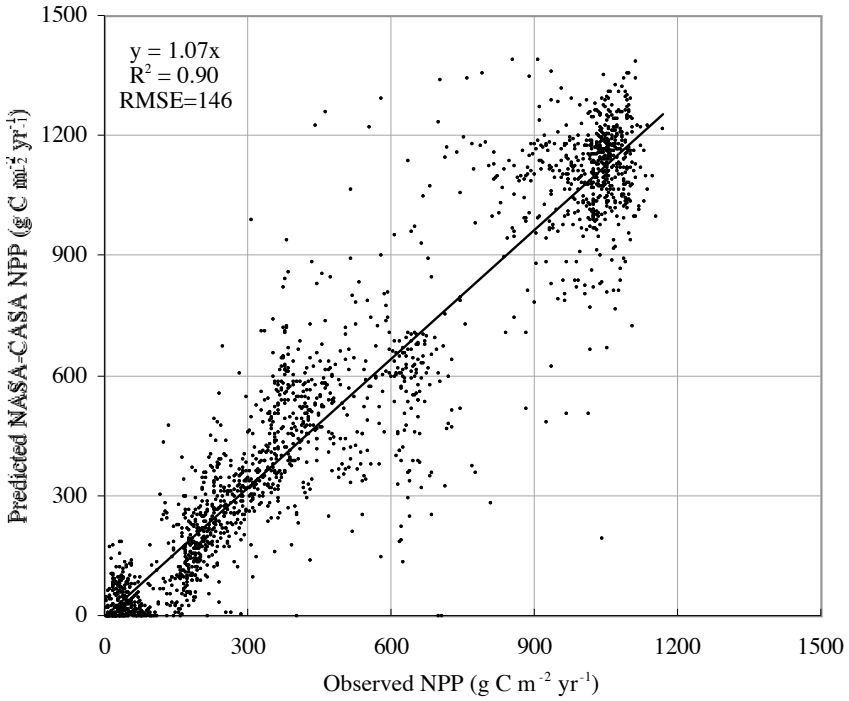

Figure 3. Locations of co-occurrence between anomalously low (LO) or anomalously high (HI) monthly event observations for climate inputs and NASA-CASA predicted NEP from 1982 to 1998 (a) PREC-LO and NEP-LO, (b) TEMP-HI and NEP-HI.

a.

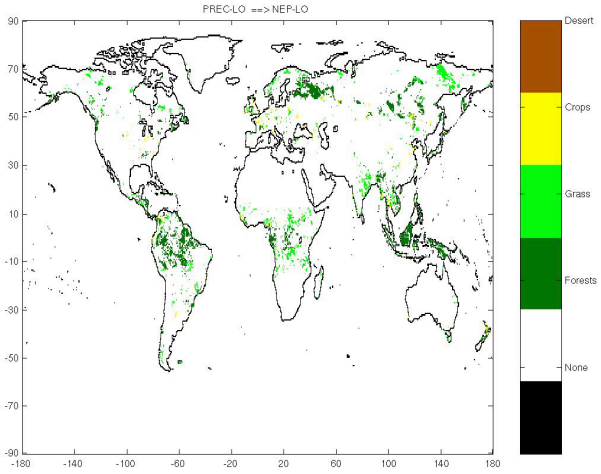

b.

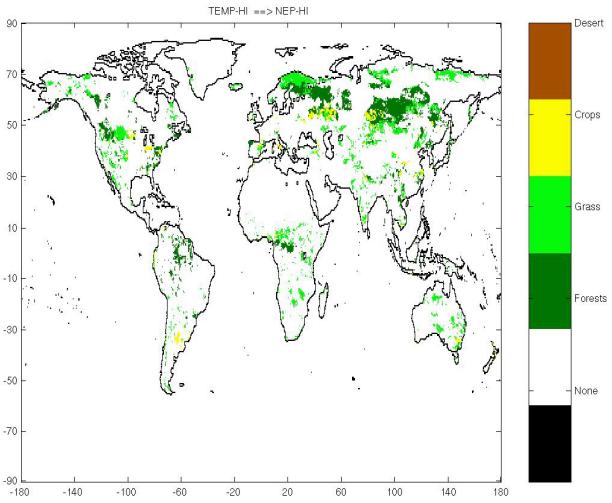

Figure 4. Time-series association of 12-month running average SOI, NINO1+2, and AO with terrestrial NPP anomalies at $r>0.4$ for selected areas of the (a) eastern Brazil, (b) southwestern United States, and (c) southern Scandinavia.

a. 5° S, 50° W , r = +0.85

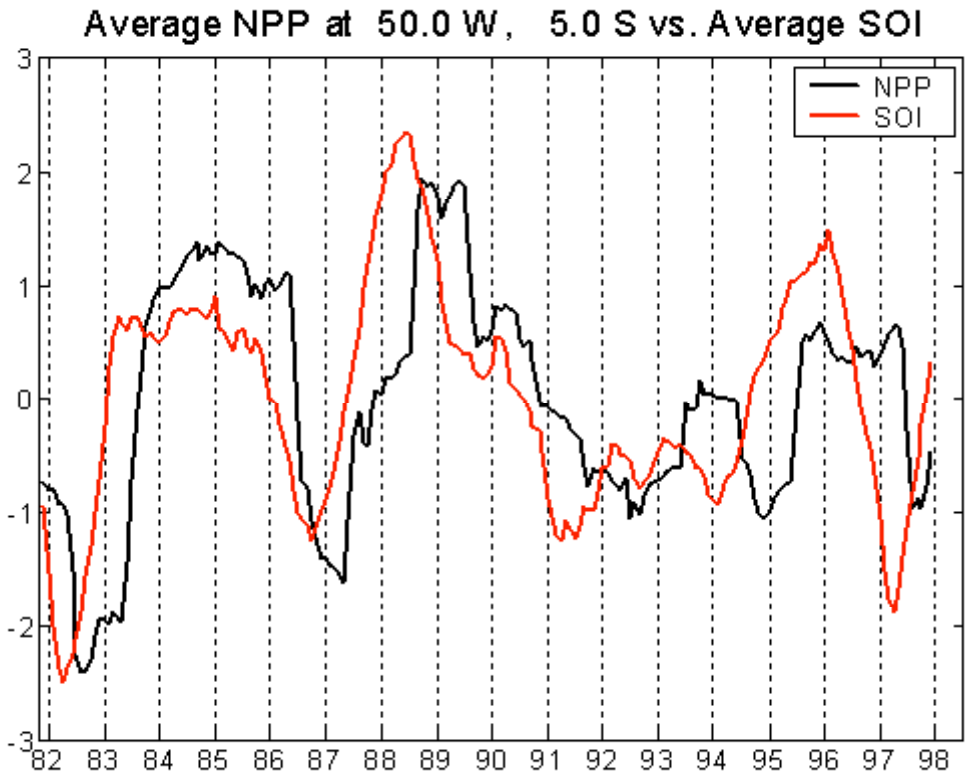

b. 28º N, 105º W, , r = -0.67

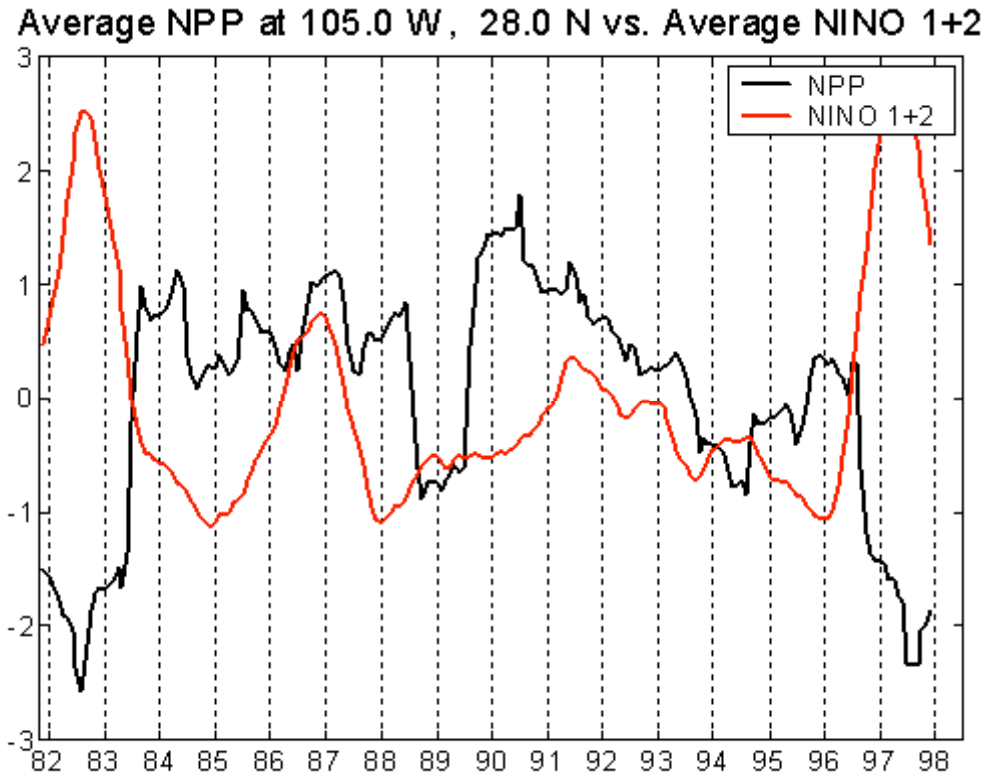

c. 60° N, 15° E, r = +0.49

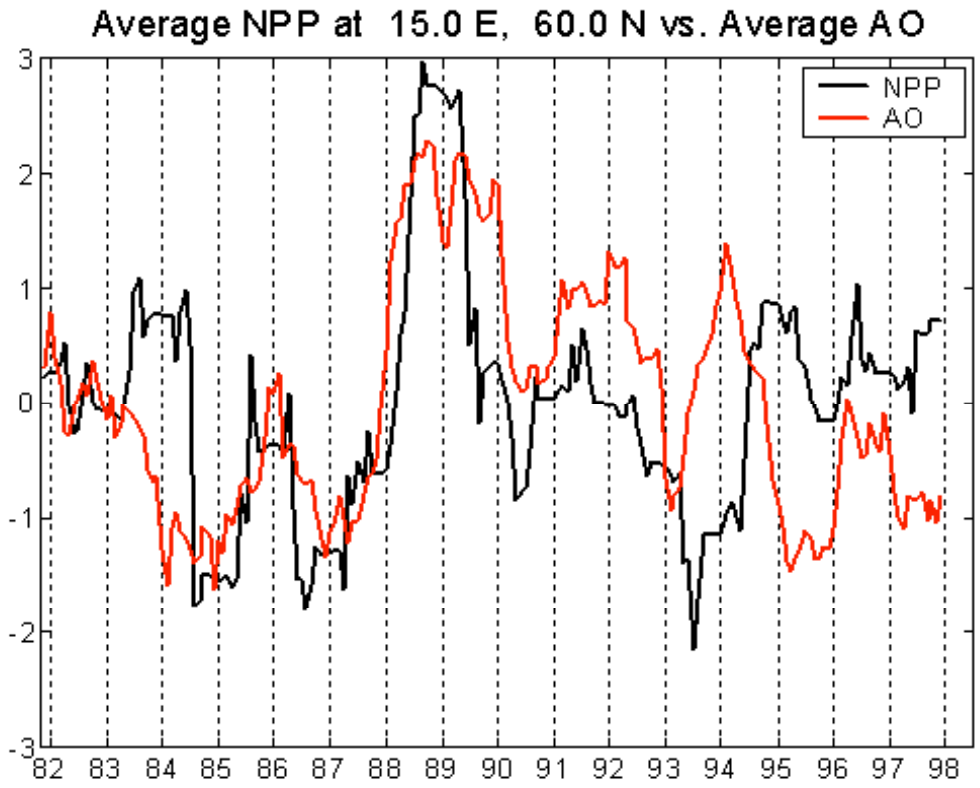

Figure 5. Global associations of SOI, NINO1+2, and AO indices with predicted terrestrial NEP (1982-98). (a-c) Areas correlated at $r > 0.34$, (d-f) Phase shifts (in months) for the strongest associations shown in maps a-c.

a.

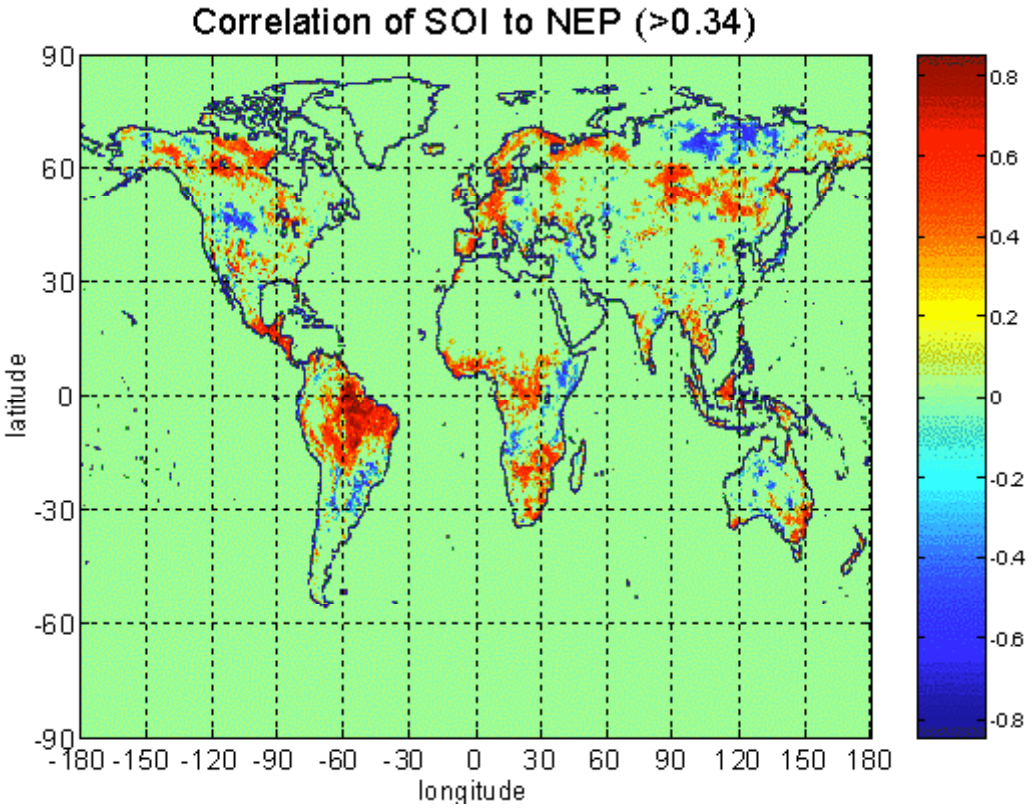

b.

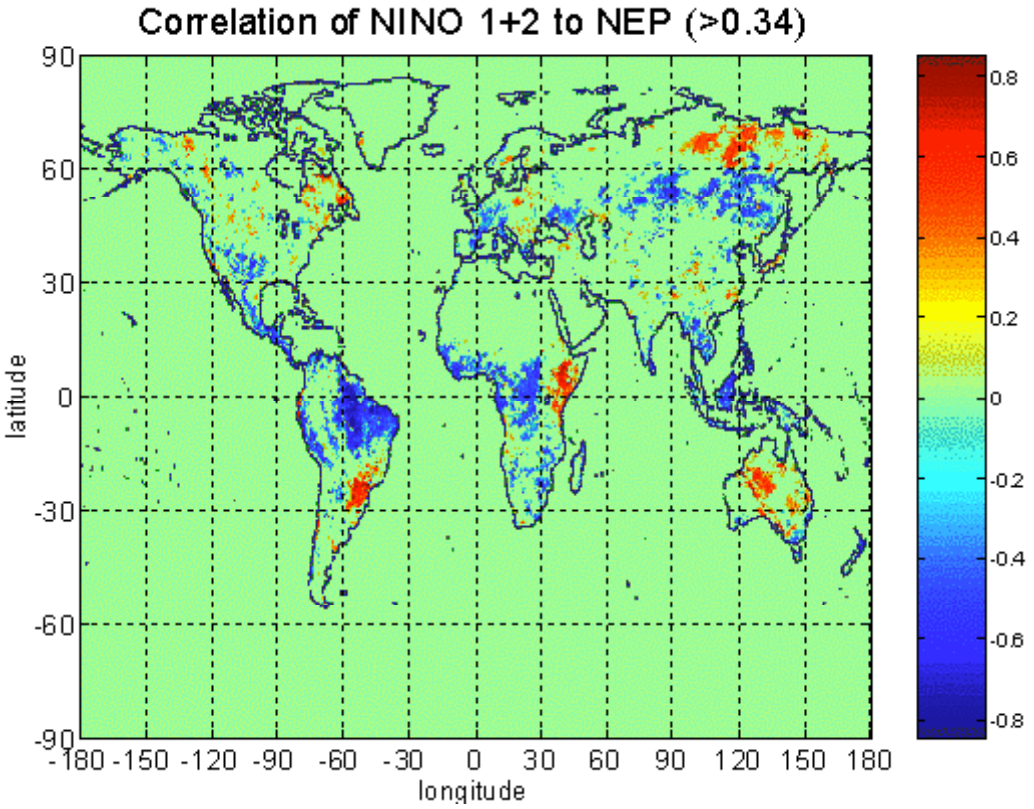
Correlation of NINO 1+2 to NEP (>0.34)
90
60
30
0
-30
-60
-90
latitude
-180 -150 -120 -90 -60 -30 0 30 60 90 120 150 180
longitude
0.8
0.6
0.4
0.2
0
-0.2
-0.4
-0.6
-0.8

c.

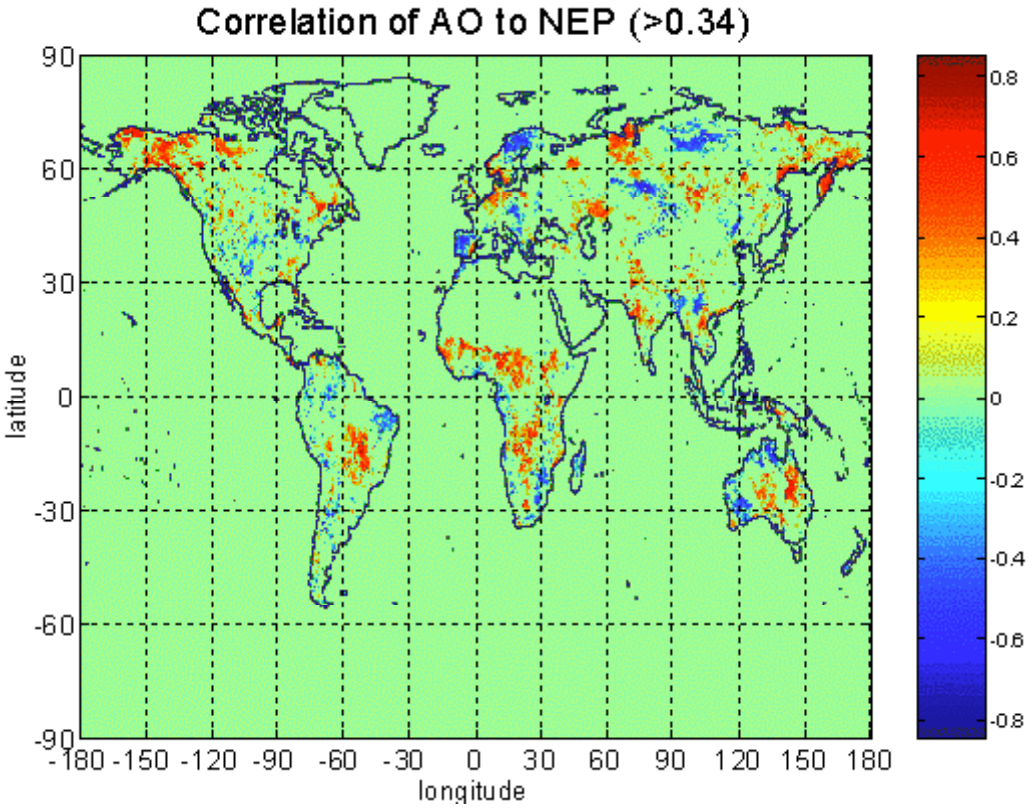
Correlation of AO to NEP (>0.34)
90
60
30
0
-30
-60
-90
latitude
-180 -150 -120 -90 -60 -30 0 30 60 90 120 150 180
longitude
0.8
0.6
0.4
0.2
0
-0.2
-0.4
-0.6
-0.8

d.

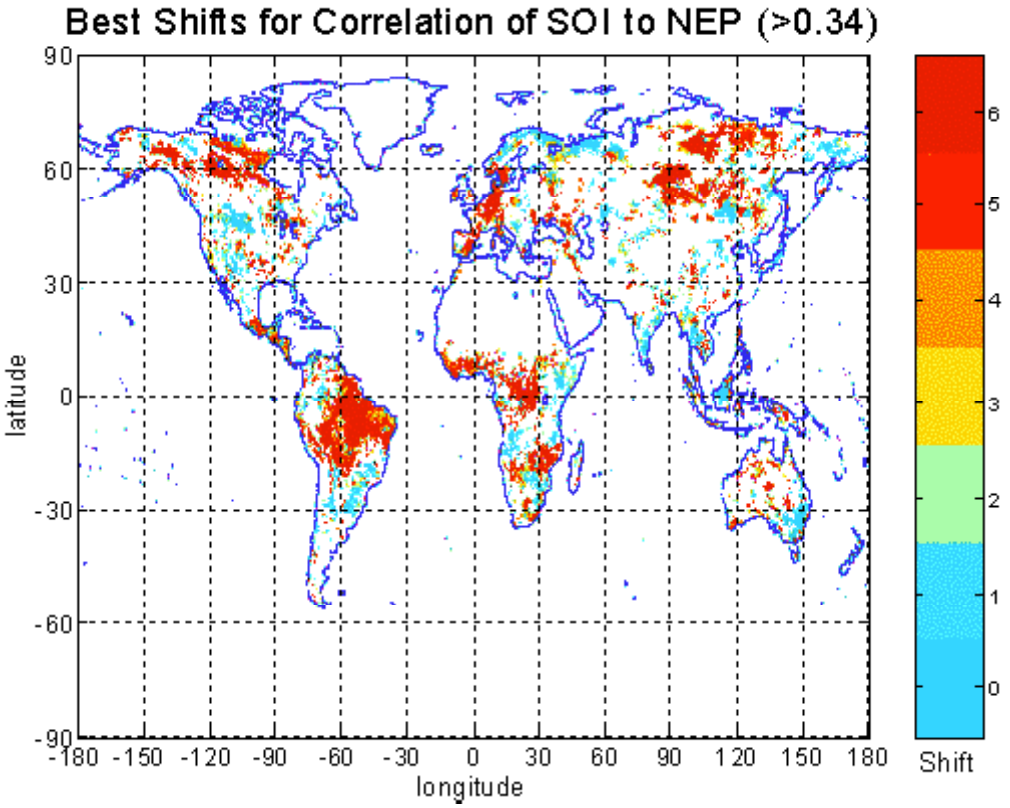
Best Shifts for Correlation of SOI to NEP (>0.34)
90
60
30
0
-30
-60
-90
latitude
-180 -150 -120 -90 -60 -30 0 30 60 90 120 150 180
longitude
6
5
4
3
2
1
0
Shift

e.

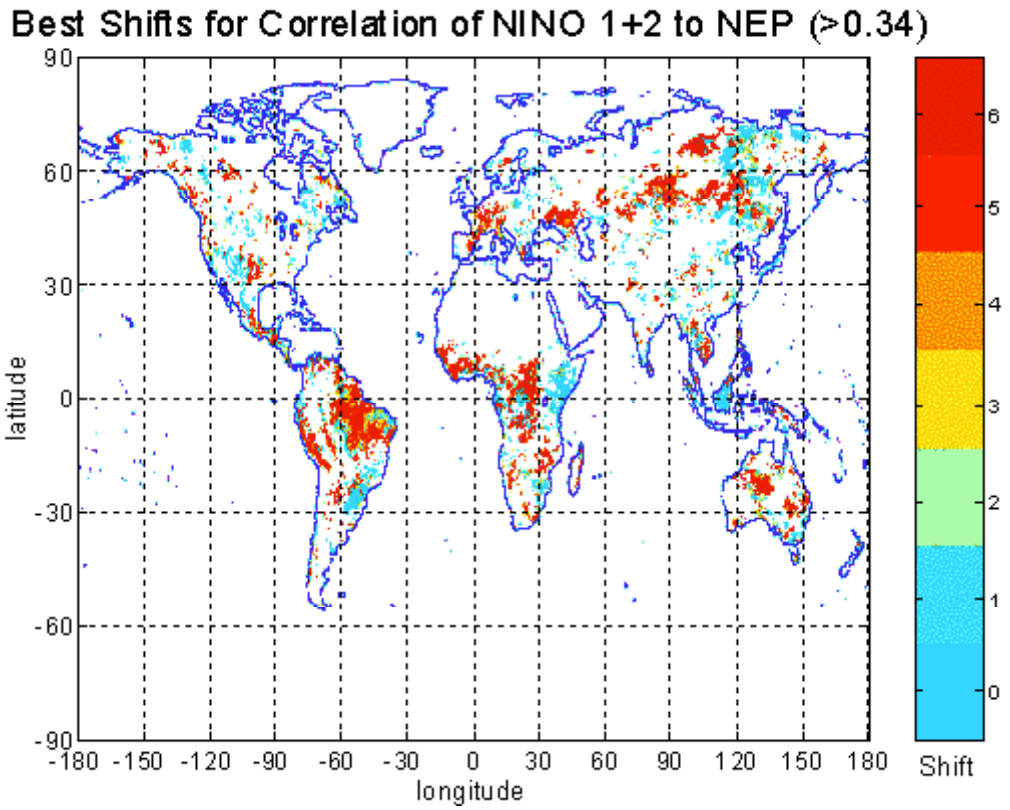
Best Shifts for Correlation of NINO 1+2 to NEP (>0.34)
90
60
30
0
-30
-60
-90
latitude
-180 -150 -120 -90 -60 -30 0 30 60 90 120 150 180
longitude
6
5
4
3
2
1
0
Shift

f.

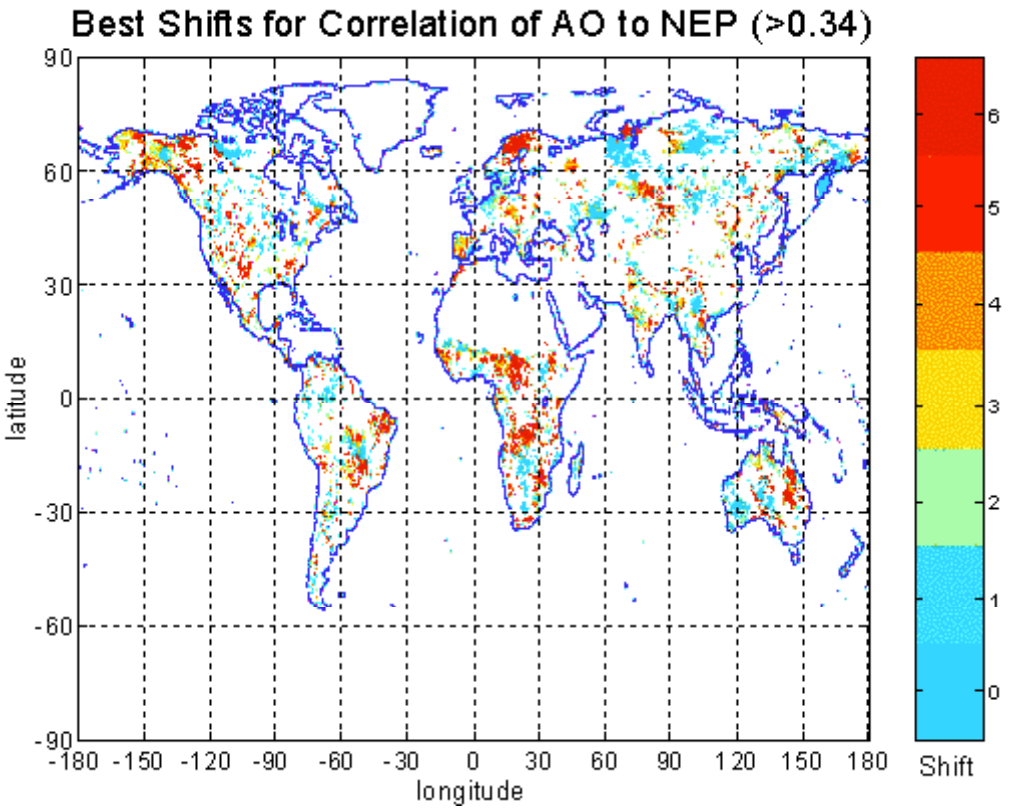
Best Shifts for Correlation of AO to NEP (>0.34)
90
60
30
0
-30
-60
-90
latitude
-180 -150 -120 -90 -60 -30 0 30 60 90 120 150 180
longitude
6
5
4
3
2
1
0
Shift